Article

Human versus Bovine Serum Albumin: A Subtle Difference in Hydrophobicity Leads to Large Differences in Bulk and Interface Behavior

Ralph Maier, Madeleine R. Fries, Cara Buchholz, Fajun Zhang,* and Frank Schreiber

ACCESS | Metrics & More | Article Recommendations | SI Supporting Information

ABSTRACT: The protein human serum albumin (HSA) is able to readily crystallize in the presence of trivalent cations, whereas this is not the case for the homologous protein in cattle, bovine serum albumin (BSA), although both have analogous functions as well as similar physicochemical properties. To understand the underlying interactions and mechanisms, we investigated their bulk phase behavior with $CeCl_3$ by visual inspection, optical microscopy, and small-angle X-ray scattering (SAXS). The results reveal that both proteins undergo reentrant condensation and liquid−liquid phase separation (LLPS). However, the LLPS binodal for HSA shifts toward lower protein concentrations than that for BSA, indicating a stronger intermolecular attraction in HSA solutions at the same compositions, consistent with SAXS measurements. Moreover, crystallization occurs within the condensed regime of HSA, but no crystallization was observed for BSA. Adsorption studies at a hydrophilic SiO_2 surface demonstrate that both systems show reentrant adsorption with a higher amount of adsorbed BSA, likely due to enhanced cation-mediated interactions and/or hydrogen bonds. We conclude that the higher surface hydrophobicity of HSA could explain the experimental observations. These additional hydrophobic interactions not only strengthen the attraction between the proteins but also provide directional and specific protein−protein contacts, which are favored for protein crystallization. This work further demonstrates the sensitivity and complexity of protein interactions in solution: subtle differences in molecular structure lead to a dramatic change in their phase behavior. Generalization of these findings can pave the way toward, e.g., better drug design and improve medical treatment.
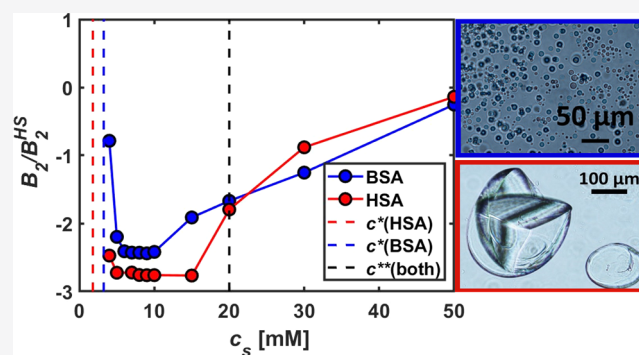
INTRODUCTION

Crystallization of macromolecules, e.g., proteins, is relevant in many fields such as pharmacology or structural biology. Although much effort is put into this research, the underlying mechanisms and interactions triggering crystallization are until now not fully understood. To elucidate the question which intermolecular interactions are required for crystallization, we performed systematic investigations on the interactions in aqueous HSA as well as in BSA solutions in the presence of solely multivalent cations as additives since only the former were reported to crystallize.

Serum albumin is the most abundant protein in the bloodstream with a physiological concentration of roughly 40 mg/mL.[1] In general, plasma proteins have two key physiological functions: maintaining the fluid balance by virtue of their colloid osmotic pressure and serving as carriers of small molecules.[2] Each mammal has its own albumin version (e.g., human serum albumin (HSA) for humans and bovine serum albumin (BSA) for cattle) since the respective primary and tertiary structures underwent a different evolution within the respective species.[3] Universally, however, the heart-shaped

serum albumin molecules are formed by three homologous domains (I, II, and III), each of which consists of two subdomains of similar structural motifs.[3,4] The subdomains IIA and IIIA contain hydrophobic cavities, which are mainly responsible for ligand binding.[3,4] Several structural features are conserved in all mammalian serum albumins such as the highly helical tertiary structure and the characteristic pattern of the 17 disulfide bridges, indicating a canonical structure.[3] Due to their important role in the body, the binding to different ligands and the phase behavior of serum albumin were and still are investigated in great detail.[1,4−16] In numerous scientific studies, however, BSA is used instead of HSA because of its easier accessibility, and the subsequent results are transferred to HSA.[3] While the two homologues do indeed share multiple

similar properties, there are also vital differences, since HSA is, for example, thermally more stable than BSA as well as more hydrophobic.[17,18]

Several of the different properties between the homologues can be explained with their structural differences and the resulting interactions. Regarding the primary structure, mature HSA contains 585 amino acids, whereas BSA contains only 583 amino acids.[3] In combination with slight differences in their sequence, this results in the fact that HSA and BSA only have 75.8% sequence identity.[3] Therefore, changes in the primary structure can be found, which are highly correlated with the evolution of the respective species.[3] Although there is a large degree of similarity between BSA, HSA, ESA (equine serum albumin), and LSA (leporine serum albumin), a number of differences in the binding pockets and especially variations in the respective surface structures and charge distributions were found.[3]

From a colloidal point of view, HSA and BSA are both globular proteins with a net negative charge at neutral pH.[19] They are not only of physiological interest but also considered as model proteins and used for studies investigating protein adsorption, protein−protein interaction, gelation, or crystallization.[10−13,20−23]

In previous work, it was established that trivalent salts induce a rich phase behavior, similar to that shown in Figure 1,
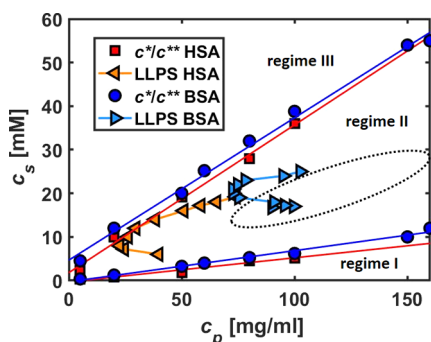
Figure 1. Phase diagram of HSA-CeCl$_3$ (red) and BSA-CeCl$_3$ (blue). Both phase diagrams were determined at 21 °C. The straight lines corresponding to $c*$ and $c**$ are fits to the respective values determined by visual inspection. Note that the experimental data for LLPS (triangles) include only the determination of protein concentration within the dilute phase at different c_s, since we focus on the minimum protein concentration needed for LLPS (onset) in BSA and HSA solutions in the presence of CeCl$_3$. The determination of the complete LLPS loop would require the determination of the salt and protein partitioning within the respective liquid phases. A hypothetical complete LLPS loop for BSA is drawn as black dotted ellipse based on refs 11, 22, 27 (which used other conditions).

and possibly even crystallization of globular proteins.[10−13,20,22−26] In this context, crystallization of HSA with YCl$_3$ and CeCl$_3$ was observed, but no crystallization of BSA in the presence of multivalent salts was reported.[10,12,13,19,20,22,24,27] To investigate this dissimilar crystallization behavior and the underlying interactions, in this work, we systematically studied the bulk phase behavior of HSA and BSA in the presence of CeCl$_3$ by visual investigation, optical microscopy, and small-angle X-ray scattering (SAXS). In addition, we studied the adsorption behavior of these two systems at a solid−liquid interface to further evaluate the interactions of these two homologous proteins to obtain better

understanding about why HSA crystallizes in the presence of multivalent cations, whereas BSA does not.

■ EXPERIMENTS AND METHODS

Materials and Sample Preparation. The proteins and the salt used were purchased from Sigma-Aldrich, now Merck, and used as received. The purities were 97% for HSA (product no. A9511), 98% for BSA (product no. A7906), and 99.99% for CeCl$_3$ (product no. 429406). Stock solutions were prepared by dissolving the protein and salt in deionized (18.2 MΩ), degassed Millipore water. The concentration of the protein solutions was determined with an ultraviolet−visible (UV−vis) spectrophotometer (Cary 50 UV−vis spectrometer, Varian Technologies) using an extinction coefficient of 0.531 mL mg^{-1} cm^{-1} at a wavelength of 278 nm for HSA and 0.667 mL mg^{-1} cm^{-1} for BSA.[28] All samples were prepared by mixing the required amount of deionized, degassed Millipore water, protein stock solution and salt stock solution. All samples had a pH (between 6.2 and 6.9) above the respective pI of the proteins, measured with a pH meter from Mettler Toledo (Germany). No additional buffer was used to avoid the effect of co-ions. All samples were prepared and investigated at 21 ± 1 °C.

Determination of the Phase Diagram. The phase diagrams of BSA and HSA with CeCl$_3$ were determined by visual inspection. Samples of protein concentrations (c_p) at 5, 20, 50, 80, and 100 mg/mL were prepared for HSA and c_p = 5, 20, 50, 60, 80, 100, 150, and 160 mg/mL for BSA at varying salt concentrations (c_s). The mean c_s of the last clear and first turbid or last turbid and first clear sample is referred to as $c*$ or $c**$, respectively. The respective $c*$ and $c**$ phase boundaries (with $c* < c**$) are plotted in Figure 1.

The dilute branches of the LLPS binodals (triangle markers in Figure 1) were determined by UV−vis spectroscopy. Samples were prepared with two different c_p, i.e., with c_p = 150 and 160 mg/mL for BSA, and with c_p = 80 and 100 mg/mL for HSA, and varying c_s to ensure reproducibility. Since the binodals thus obtained for different protein/salt conditions are nearly identical within one protein, only one data set is shown for better clarity. The macroscopic phase separation was ensured by visual inspection (see exemplarily Figure S1 for BSA). For the binodal determination, the samples tubes were centrifuged for 8 min with 5000 x g to separate the dilute and the dense phase. Afterward, the concentration of the dilute phase was determined with a UV−vis spectrophotometer. Note that the complete LLPS binodal needs to consider both protein and salt partitioning in the two liquid phases, which leads to an ellipsoidal-shaped closed loop in regime II (see refs 11, 22, 27). In this work, we focus on the minimum protein concentration needed for LLPS in BSA and HSA solutions in the presence of trivalent salt; thus, only the protein concentrations in the dilute phases were determined.

Optical Microscopy. An optical microscope (Axio Scope.A1, Carl Zeiss AG) was used for optical investigations of the samples. Images were recorded with a camera (Axio-Cam ICc5, Carl Zeiss AG) using the software ZEN Lite 2012. Samples were prepared in a separate tube. Afterward, 25 μL were transferred into a Gene Frame (1 × 1 cm with a thickness of 0.25 mm from Thermo Scientific, Germany) on a glass slide and subsequently covered with a cover slide.

For crystallization experiments, multiple conditions were investigated to check for the optimal crystallization conditions. Samples were directly transferred into the Gene Frame and after 14 days, the presence or absence of crystals was recorded. This study was carried out for samples containing 20, 35, 50, and 80 mg/mL HSA with varying CeCl$_3$ concentrations. For BSA solutions, the samples used for the determination of the phase diagram were kept for several weeks to monitor the crystallization behavior.

Small-Angle X-ray Scattering (SAXS). SAXS measurements were performed at the Petra III beamline P12 (Hamburg, Germany).[29] With a sample-to-detector distance of 3 m and an X-ray energy of 10 keV, a q-range of 0.03−7.3 nm^{-1} was achieved. The sample was exchanged using a flow cell. For each sample, 40 exposures of 0.045 s were checked for radiation damage and averaged. The 2D intensity pattern was azimuthally averaged to obtain the

intensity profiles. Afterward, the solvent background was measured the same way and subtracted.

Additional SAXS data were collected with a Xeuss 2.0 instrument (Xenocs, Grenoble, France) employing a GeniX 3D microfocus X-ray tube with a copper anode, using an X-ray wavelength of 0.154 nm. With a sample-to-detector distance of 1850 mm, the employed Pilatus 300K detector covered a q-range of 0.055−2.25 nm^{-1}. Quartz capillaries with a diameter of 2 mm were used for this setup. Each acquisition time was 30 min.

To determine the reduced second osmotic virial coefficient $B_2' = B_2/B_2^{HS}$ with $B_2^{HS} = 16\pi R^3/3$ being the second virial coefficient of hard spheres, the data were fitted with a sticky hard sphere (SHS) model[30] using IGOR PRO 6.37 in combination with macros provided by NIST.[31] The potential for particles with radius R is described as

$$\beta U(r) = \begin{cases} \infty & r < \sigma = 2R \\ -\beta u_0 = \ln\left(\dfrac{12\tau\Delta}{\sigma + \Delta}\right) & \sigma < r < \sigma + \Delta \\ 0 & r > \sigma + \Delta \end{cases} \quad (1)$$

with $\beta = 1/k_B T$. τ stands for the stickiness parameter and Δ denotes the width of the square well. A pertubative solution of the Percus−Yevick closure relation was used to calculate the structure factor.[32,33]

Prior to their investigation, the samples were briefly centrifuged and only the clear supernatant was examined. The protein concentration of the HSA samples was determined with the help of the binodal in the phase diagram (Figure 1) in a 10 mg/mL range and for the BSA samples, a concentration range between 40 and 50 mg/mL was assumed since the initial concentration was 50 mg/mL and no LLPS occurred for these conditions. With the specific volumes of 0.735 mL/g for BSA[34] and 0.754 mL/g for HSA,[35] the respective volume fractions were calculated. Similar to refs 33, 36, Δ was set to 0.01 σ to avoid artificial coupling with τ, the axes of the ellipsoid were fixed to $r_a = 1.8$ nm and $r_b = 6.1$ nm and the scattering length density (SLD) of the ellipsoid was set to 1.24·10^{-7} nm^{-2}. Since HSA and BSA are similar in size and shape (see Table 1), the same values are used for both proteins.

Table 1. Physicochemical Properties of BSA and HSA

	BSA	HSA
molecular weight [kDa][53,54]	67	66.5−69
hydrodynamic radius R_H [nm][53]	3.3−4.3	3.3−4.1
# amino acids[3,55]	583	585
# positive/negative residues[19]	80/91	80/89
pI[19]	4.6	4.6
charge (pH 7) [e][19]	−11	−9
overall hydropathy Ω[18]	−279.2	−230.8
secondary structure [%][14,56] (α-helix/β-sheet/β-turn)	(53/14/4)	(66/4/22)

In the limit $\Delta \rightarrow 0$, which is used here, the reduced second virial coefficient can then be calculated by

$$\lim_{\Delta \rightarrow 0} \frac{B_2}{B_2^{HS}} = 1 - \frac{1}{4\tau} \quad (2)$$

Due to aggregation or further LLPS within the samples indicated by a strong increase of intensity at low q-values (< 0.1 nm^{-1}) (see Figure 3), the model was only applied for q-values ≥ 0.1 nm^{-1}. Representative fits are plotted in Figure S2.

For protein solutions with a c_s of 1 mM, a screened Coulomb (SC) potential[37,38] was used to describe the effective interactions. According to ref 39, the axes of $r_a = 1.7$ nm and $r_b = 4.2$ nm for low c_s were used. The SLD of the ellipsoid was again set to 1.24·10^{-7} nm^{-2}, the temperature to 293 K, the monovalent salt to 0.006 M (having the same Debye length as 1 mM CeCl$_3$) and the volume fraction was calculated similarly to the SHS fits. Similar to the

procedure above, the model was applied only for q-values ≥ 0.1 nm^{-1}. The respective fits can be seen in Figure S3.

Quartz Crystal Microbalance with Dissipation (QCM-D). Protein adsorption measurements were performed with a Q-Sense Analyzer (Biolin Scientific, Sweden).[40−42] The samples were mixed and 5 mL of the protein/salt mixtures was pumped into a previously degassed Milli-Q water-calibrated QCM-D cell. The signal of the adsorption process was recorded for approximately one hour and the cell was subsequently rinsed by Milli-Q water to detect irreversibly bound proteins. Native silica-coated quartz sensors (product no. QS-QSX303 from Quantum Design, Germany) were used as substrates for this setup. The flow cell was inverted during the complete measurement and cleaning, i.e., with the substrate on top of the solution, to avoid sedimentation effects. After each measurement, the flow cell was cleaned in situ in three steps with 2% Hellmanex, ethanol, and water. The QSoft software was used for data collection while Dfind and QTools (Biolin Scientific) were used for data analysis and figure generation. Since the dissipation (D) was > 0, a viscoelastic (Voigt) model was applied for the data collected.[43,44] More details regarding data analysis and fitting parameters can be found in refs 12, 13, 20. Each adsorbed protein layer thickness d at the solid−liquid interface is the mean of at least three individual measurements to check for reproducibility and to estimate the error of the measurement. Thus, the error bars indicate the respective standard deviations.

■ RESULTS AND DISCUSSION

Phase Diagram. As a first step, the respective phase diagrams were established. Figure 1 shows experimental phase diagrams of HSA and BSA in the presence of CeCl$_3$. While parts of the phase diagram of HSA-CeCl$_3$ were already discussed in a previous work,[10] the BSA system was newly established in the context of this study. One can see that HSA and BSA both show a rich phase behavior including reentrant condensation (RC) and liquid−liquid phase separation (LLPS) in the presence of CeCl$_3$ (see Figure 1). This rich phase behavior has been established for net negatively charged, globular proteins in the presence of multivalent salts, but can also be found in solutions of positively charged proteins and negatively charged polyoxometalates.[10,12,13,20,22,23,25,45,46] The proteins initially repel each other by virtue of their negative charge, forming a clear and stable solution (regime I). By increasing c_s and crossing c^*, the proteins macroscopically aggregate/condense, which leads to an optically turbid solution. In this turbid solution, the multivalent cations bind to the carboxyl groups at the protein surface, therefore weaken the repulsive forces between the initially negatively charged proteins, and the effective attraction is strong enough to cause protein condensation (regime II).[25,45] By further increasing c_s, above c^{**}, the attractive interactions between the proteins become weaker and the solution becomes clear and stable again (regime III), which is defined as RC.[19,24,25,45] The driving force for this behavior was found to be an effective charge inversion of the proteins.[25,45] In regime II, a metastable LLPS regime can occur, if the effective attractive protein−protein interactions are sufficiently strong.[11,47] Samples prepared under conditions inside this LLPS regime phase separate into a dense and a dilute liquid phase.

The comparison of the HSA with the BSA phase diagram shows a shift of the LLPS binodal about three-fold higher protein concentrations for BSA (72 vs 22 mg/mL), indicating stronger attractions in HSA than BSA solutions under the same condition. The slight shift of c^* and c^{**} can be explained by the fact that BSA has two acidic residues more than HSA, meaning more negatively charged (see Table 1),[19] and thus

more cations are required to balance the electrostatic repulsion and induce the phase transitions.

Crystallization. After establishing the phase boundaries and the LLPS binodal, we focused on protein crystallization and the crystallization conditions within the phase diagram. Crystallization of HSA in the presence of multivalent salt has been reported in the literature, but so far not for BSA.[10,12,13,19,20,22,24,27] The conditions of HSA-CeCl$_3$ crystals or their absence after 14 days for numerous conditions are plotted in Figure 2. Representative images of HSA crystals
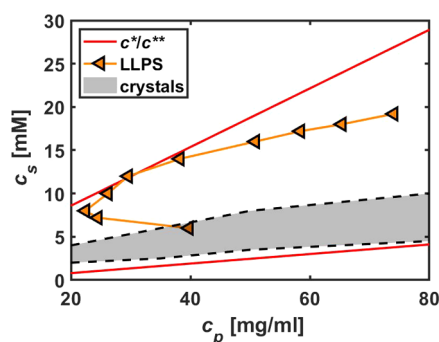
Figure 2. Conditions of HSA-CeCl$_3$ crystallization recorded after 14 days; 20, 35, 50, and 80 mg/mL HSA samples were investigated at varying c_s. Conditions which showed crystals are shaded gray within the HSA-CeCl$_3$ phase diagram.

grown under different conditions are shown in Figure S4. It is clearly visible that crystallization mainly occurs in regime II, especially in the lower half, including both conditions outside and inside the LLPS area. A detailed study of the role of LLPS on nucleation has been performed for this system and the reader is referred to ref 10 for more information. The absence of crystallization in the upper part of regime II will be discussed in the Discussion section.

In contrast to HSA, none of the BSA samples crystallized. In fact, no BSA crystals were observed for any set of conditions studied in our work. This is also true for BSA with other multivalent salts, namely, YCl$_3$, HoCl$_3$, LaCl$_3$, LaI$_3$, and YI$_3$ (see exemplarily SAXS data of BSA-LaI$_3$ in Figure S5), and thus apparently a rather general effect.

Effective Bulk Interaction Characterized by SAXS. As a next step, the effective intermolecular bulk interactions resulting in the different crystallization behavior were characterized by SAXS. Figure 3a shows raw SAXS data of a set of samples containing 50 mg/mL HSA and varying c_s and Figure 3b shows the corresponding data for 50 mg/mL BSA. In both figures, first, an increase in the low q intensity can be observed upon increasing c_s, indicating increasing attractive interactions. Simultaneously, the correlation peak at $q \approx 0.5$ nm^{-1}, which denotes a dominant electrostatic repulsion between the particles in solution, vanishes. At moderate c_s, a maximum of the low q-intensity is visible, and for a high c_s, it decreases again. This behavior corresponds well with the phase diagrams shown in Figure 1, in which the three different regimes are observed. In the condensed regime (regime II), the inter-particle attraction is strong enough to induce protein aggregation/condensation. The trend of SAXS profiles observed in Figure 3 is consistent with previous works investigating intermolecular interactions of RC systems.[12,23,33,36]
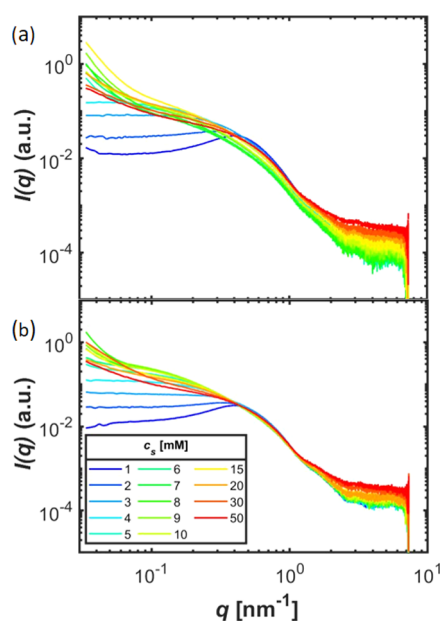
Figure 3. SAXS intensity curves of samples containing (a) 50 mg/mL HSA and (b) 50 mg/mL BSA and varying CeCl$_3$ concentrations of 1−50 mM.

To quantify these observations, B_2'-values from the model fit are plotted in Figure 4. B_2' is a measure of the intermolecular interactions of a system. $B_2' < 0$ implies a net attraction, whereas $B_2' > 0$ represents a net repulsion. The B_2'-values slightly decrease for both proteins upon increasing c_s, reach a minimum (which is negative, hence attractive) in regime II and increase again in regime III. Unfortunately, the model is physically limited to attractive interactions, hence, the B_2'-
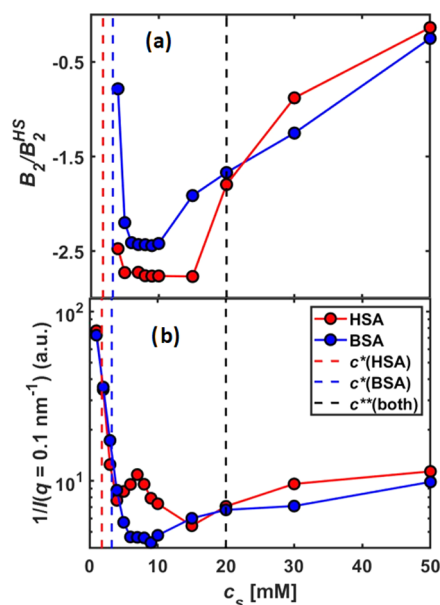
Figure 4. (a) Reduced second virial coefficients B_2/B_2^{HS} and (b) $1/I(q{\to}0)$-behavior of the raw SAXS data of HSA and BSA samples with $c_p = 50$ mg/mL and varying c_s presented in Figure 3. The respective phase boundaries are also plotted. c^{**}(both) represents the c^{**} boundary, which is identical for HSA and BSA. For all images, the errors are typically at least one order of magnitude smaller than the respective data values and therefore not plotted for clarity.
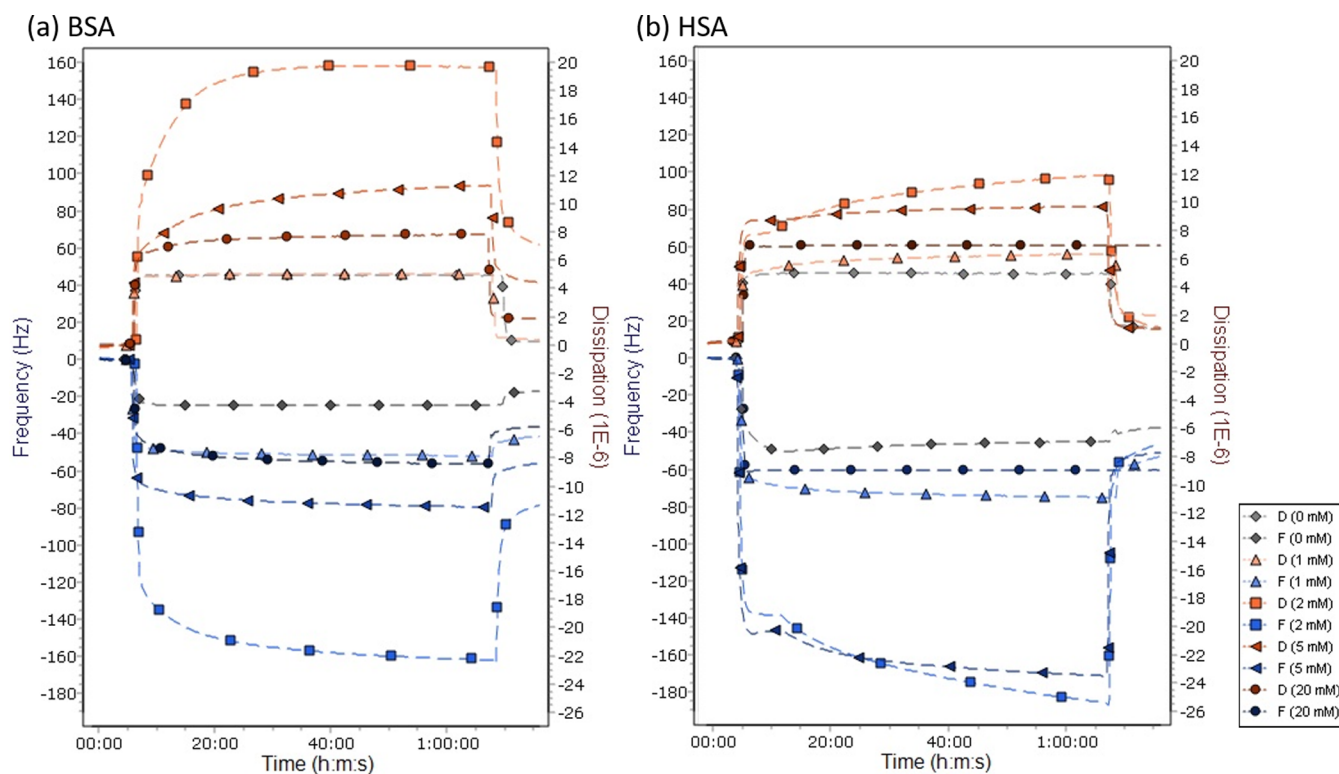
Figure 5. Raw QCM-D data of samples containing (a) 20 mg/mL BSA or (b) 20 mg/mL HSA with different c_s values. The frequency of the 9th overtone is plotted in blue, whereas the dissipation is plotted in red. For clarity, only one condition of each regime is plotted. The different c_s values represent all individual regimes in the phase diagram.

values of regime I, approaching c^*, could not be determined by this procedure. However, the results are in good agreement with the phase diagrams shown in Figure 1, showing a reentrant strength of attraction with the strongest attractions in regime II. Comparing HSA with BSA shows that HSA has lower B_2'-values and therefore stronger attractions in regime II while this trend is opposite when crossing c^{**}.

For further understanding of the effective interactions, a model-free analysis was applied. $1/I(q \rightarrow 0)$, i.e., the inverse intensity at low q-values (close to 0), is also a measure of the intermolecular interactions of a sample, since it is proportional to the isothermal compressibility of the system investigated and the respective second osmotic virial coefficient B_2.[48] The respective curves can be found in Figure 4b. Since it is a model-free analysis, it is not limited to attractive conditions like the SHS analysis, but also low c_s can be investigated. Here, the sharp decrease from repulsive forces to attractive forces is visible when crossing c^*. Otherwise, they exhibit the same trend as the respective B_2'-curves with the only difference being the additional bump in the second regime for HSA. This additional increase and decrease was found to be caused by LLPS. In the virial expansion of the structure factor (eq 3), ρ is proportional to c_p, hence, a change in c_p of the measured dilute phase due to LLPS affects the $1/I(q \rightarrow 0)$-behavior and causes this bump at $c_s = 8$ mM.[33,49] These results are consistent with the phase diagrams which show LLPS for HSA at 50 mg/mL, but not for BSA (see Figure 1).

$$1/S(q \rightarrow 0) = 1 + 2B_2\rho + \dots \qquad (3)$$

As a last step of the SAXS analysis, an SC potential was fitted to the protein samples with the lowest c_s, i.e., with 1 mM CeCl$_3$ (see Figure S4), to compare the pure proteins (without or with

little salt). The curves and fits are nearly identical with the only difference being a decrease at very low q-values for BSA compared to an increase for HSA, which might stem from HSA aggregation. The net charges resulting from the fits are −14 e and −13 e for BSA and HSA, respectively. Similar to ref 19, a slightly more negative charge is obtained for BSA. These results indicate that the proteins behave similarly without (or with little) salt added, but BSA is slightly more negatively charged.

Adsorption Studied by QCM-D. In this section, the adsorption behavior of HSA and BSA solutions at a hydrophilic, negatively charged SiO$_2$ surface is presented to further elucidate the strength and nature of the interactions of these two proteins. Figure 5 shows the raw data of samples containing a protein concentration of 20 mg/mL and different salt concentrations (0, 1, 2, 5, and 20 mM). Similar frequency decreases (roughly proportional to the amount of adsorbed protein) can be seen for both BSA and HSA samples, whereas the dissipation increases are more pronounced for BSA. Figure 6 shows the respective calculated thicknesses based on a full fit following ref 12. A complex adsorption behavior is recorded for both HSA and BSA. Initially, an increase in adsorbed protein layer thickness d can be observed until a maximum value is reached. Increasing c_s further results for both proteins in a decrease in d until the adsorption layer saturates in regime III, known as reentrant adsorption (RA).[12,13,20] This result is in line with previous work on similar systems.[12,13,20,50] The observation of a maximum adsorbed amount is also consistent with the bulk data, which show a maximum of attraction in the second regime. Figure 6b presents the irreversibly adsorbed protein layer after rinsing for both systems. The overall thickness is significantly reduced, but the similar trends remain.
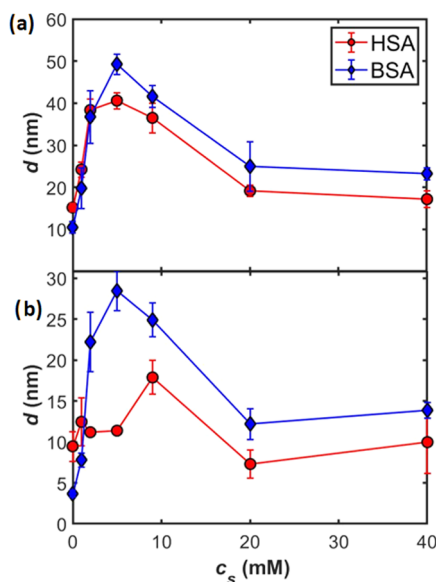
Figure 6. (a) Adsorbed protein layer thickness (d) of 20 mg/mL BSA (blue diamonds) and HSA (red circles) on a SiO$_2$ quartz calculated from the raw data exemplarily shown in Figure 5 with the Kelvin–Voigt model and (b) data after subsequent rinsing with water. Each data point is the mean of at least three individual measurements. The error bars indicate the respective standard deviation. Note that 20 mg/mL is outside and just at the border of the LLPS region for BSA and HSA, respectively (see text for details).

With zero or low c_s, the adsorption thickness d is slightly higher for HSA than that for BSA, which is expected as HSA is more hydrophobic and has less surface charge. This observation is consistent with the literature: Kurrat et al. reported that in HEPES and PBS buffer, HSA has a thicker adsorption layer than BSA.[51] The interesting observation is that in regimes II and III, more BSA adsorbs at the surface than HSA. If we only consider the bulk behavior, it may seem surprising at first glance that more BSA are adsorbed at the surface than HSA including the irreversible bound proteins (see Figure 6) since weaker intermolecular interactions are observed in bulk for BSA. This can be explained, though, by the fact that BSA is more hydrophilic than HSA,[18] hence, more BSA proteins adsorb at the hydrophilic surface. In addition, BSA is more negatively charged than HSA (see Table 1),[19] In our previous work on protein adsorption in the presence of multivalent cations (see refs 12, 13, 20, 50), we have demonstrated that indeed the cation-mediated interactions lead to an enhanced adsorption at hydrophilic interfaces, i.e., the trivalent cations preferentially adsorb to the natively negatively charged silicon wafer. Further, the specific interactions between these adsorbed cations and the carboxyl groups on the protein surface enhance the protein adsorption. Therefore, as BSA has two acidic residues more than HSA,[19] BSA provides more possible binding sites for the cations and thus induces stronger binding, and possibly denser packing, to the surface, and the cation-mediated adsorption leads to a thicker layer for BSA compared to HSA in regimes II and III.

Note that all samples used in the QCM-D were below the LLPS binodal, and were thus not phase separated. In a recent publication, we have shown that the adsorption is enhanced inside or close to the LLPS binodal.[20] Since the HSA conditions are located just outside the binodal compared to the BSA conditions, which are far away from the binodal, one

would expect a higher d for the HSA samples. Since actually the opposite is the case, we attribute this to strong cation-mediated adsorption and/or hydrogen bonds of BSA with the substrate. Another aspect one has to take into account is that QCM-D also detects water in the adsorbed layer. Since BSA is more hydrophilic,[18] more water molecules should be coupled to the protein and hence an increased thickness should be observed compared to HSA.

As shown in Figure 5, QCM-D provides also the dissipation parameter D, which is a measure for the viscoelastic properties of the media investigated. In regime II, D is roughly twice as high for BSA as for HSA (see Figure 5), suggesting a denser and stiffer (i.e., more "solid-like") layer for HSA. In accordance with this, the viscosity of the HSA layer is approximately twice of the BSA layer. A high viscosity may be due to strong protein–protein interactions and may correspond to binding and cluster formation,[52] which is consistent with the SAXS measurements in Figure 4.

Discussion. Due to the highly complex structure of globular proteins, different properties and parameters simultaneously influence their bulk and interface behavior. To provide a comprehensive discussion, the following section highlights similarities as well as differences of HSA and BSA deducing the key mechanism triggering the different bulk (crystallization) and adsorption behavior of BSA versus HSA. Here, the main focus lies on their secondary structure, the binding behavior of various ligands, and the respective behavior at interfaces as well as in bulk. Some physicochemical parameters are listed in Table 1.

HSA was found to bind lanthanides in blood serum.[57] The ions of cerium and the transition-metal ions of yttrium were found to bind at negatively charged glutamate residues of HSA, forming intermolecular crystal contact sites.[10] Since each HSA molecule binds four ions, 15.4 % of its surface area is responsible for cation binding within a crystal.[10] We note that the role of the multivalent cations on protein crystallization is similar to the one of anionic calixarene scaffolds, which are used to mold to cationic proteins, and induce oligomerization and crystallization.[58] Further studies on BSA show that the lanthanide metal ions Yb^{3+} and Gd^{3+} bind to BSA with four equivalent affinity sites in a pH range of 6−7 (with association constants Yb^{3+}-BSA ≫ Gd^{3+}-BSA).[59] The authors conclude that the Yb ions bind to histidine while the binding site of the Gd ions is not fully clear.[59] Hence, both proteins easily bind lanthanide cations, which is also revealed in the RC phase diagrams due to ion binding and bridging.[19,24,60]

Regarding their secondary structure, Blaber et al. report that the helix propensity depends strongly on the hydrophobic effect of the respective amino acids, which stabilizes the helical structure.[61] Since HSA has a higher fraction of α-helices, it is reasonable to conclude that more or stronger hydrophobic interactions are present compared to BSA. Akdogan et al. actually report that the differences in hydrophobicity between the albumins often occur at surface-exposed residues, which is crucial for the rationalization that HSA is less hydrophilic than BSA as evidenced by their hydropathy Ω (see Table 1).[18] In terms of intermolecular interactions, HSA is supposed to be better at attracting and binding hydrophobic and amphiphilic ligands.[6,18] In contrast, interactions with water and hydrogen bonding are hindered compared to BSA. These findings are consistent with the adsorption data presented (see Figure 6).

In addition to the LLPS binodal shift, the biggest difference in the respective bulk behavior is that HSA crystallizes in the

presence of multivalent cations and BSA does not. George and Wilson stated in an empirical study that the intermolecular attractions have to be in a relatively narrow range for crystal nucleation.[62] According to this study, the optimum crystallization conditions are around or slightly below the critical point of LLPS. Vliegenthart and Lekkerkerker calculated the B_2'-value at the critical point to be approximately -1.5.[47] This empirical study was rationalized by a kinetic model for the growth rates of protein crystals. Schmit and Dill assume that the protein can bind to the crystal surface in two ways: productively (in the correct crystal orientation and alignment), or nonproductively (in a noncrystalline orientation).[63] Crystal growth only occurs when proteins bind productively.[63] They propose that too strong attractions lead to nonproductive attachment of proteins to the crystals.[63] Since LLPS can be observed for both HSA and BSA in the presence of multivalent salts (see Figure 1) and both proteins show B_2'-values ≤ -1.5 (see Figure 4), both proteins should theoretically have attractions strong enough to induce crystallization. However, we only monitor HSA crystals in our systems. This indicates clearly that some differences between HSA and BSA (most likely at the protein surface) do have to exist, which are responsible for this dissimilar behavior.

It is also known that an interplay between anisotropic and isotropic interactions is crucial for protein crystallization.[64,65] It seems that only ion bridging is not sufficient for serum albumin to crystallize. It is able to induce an RC bulk behavior and LLPS, but for crystallization additional forces are required. This can also be seen from the fact that some crystal contacts of HSA-Y^{3+} crystals are formed by solely protein−protein interactions,[10] which are assumed to be of hydrophobic nature. These additional intermolecular contacts are believed to aid in orienting and aligning proteins, resulting in a productive binding to promote crystallization.[63] The absence of HSA crystallization at a high c_s may be due to the high occupation of binding sites by metal ions, which could block the protein−protein contacts, or change the crystallization pathway (or crystals simply need a much longer induction time, beyond the observation time). We note in another system (BLG with YCl_3), crystallization near $c*$ and $c**$ shows different pathways.[25]

The hypothesis that the additional hydrophobic interactions of HSA drive crystallization is supported by the fact that either highly hydrophobic or highly polar surface regions were reported to have an increased probability of establishing crystal lattice contacts.[66] By increasing the hydrophobicity at the protein surface, proteins can assemble in new crystal packings.[66] Approximately 68% of the contact area in cutinase crystals is hydrophobic while around 30% of the total hydrophobic area of the protein is involved in contact formation, indicating the crucial role of the hydrophobic interactions for protein crystallization.[66] The hydrophobic patches favor protein−protein interactions and counteract the repulsive forces arising from charged functional groups, hence contributing significantly to the formation of protein crystals.[67] Further support is obtained by recent models indicating that the fraction of exposed residues in combination with their hydrophobicity plays a vital role in protein crystallization propensity.[68]

We note that, while we have not observed BSA crystallization in the presence of multivalent cations, BSA was crystallized in specific systems using poly(ethylene glycol) (PEG) as precipitant or at gas-liquid interfaces.[3,69,70] In refs 3,

69, however, BSA was further purified by removing fatty acids bound to the protein and/or eliminating dimers.[71] In ref 70, the protein was purchased from a different company, which gives no information about its purification methods, and acidic solutions (pH 4.3) were used. Hence, the degree of purification of the proteins and the aqueous environment differ compared to our system, which seemingly affects the phase behavior substantially. In our work, we have observed a variation of phase boundaries (such as $c*$ and $c**$) due to the usage of different batches, but in all batches HSA, crystallizes under certain conditions. BSA, however, never crystallizes under any experimental conditions employed by us.

■ CONCLUSIONS

In summary, we have studied the protein bulk phase behavior and the adsorption at an interface for HSA and BSA solutions in the presence of the trivalent salt $CeCl_3$. Both systems exhibit a rich phase behavior including RC and LLPS; however, only HSA crystallizes in regime II, but BSA does not. SAXS measurements confirm stronger intermolecular attractions for HSA compared to BSA solutions in regime II. Protein adsorption experiments at a hydrophilic, negatively charged SiO_2 substrate show a thicker layer for BSA in regimes II and III, which is in good agreement with the cation-mediated protein adsorption,[12,13,20,50] where the more hydrophilic BSA shows an enhanced adsorption behavior.

Although many physicochemical properties are similar (see Table 1), both bulk and adsorption results show that crucial differences between HSA and BSA exist. Especially for crystallization, an interplay of isotropic and anisotropic interactions is essential. While the multivalent cation binding and bridging induce RC and RA, hydrophobic interactions and hydrogen bonding fine-tune this behavior. Hence, the more hydrophilic BSA seems to bind more strongly to water and to negatively charged, hydrophilic surfaces, whereas the additional hydrophobic forces of HSA are able to promote crystallization. In conclusion, depending on the favorable or unfavorable binding to ligands or surfaces, the whole range of interaction types needs to be considered and accurately chosen for the desired application. These findings are of vital importance in many research areas, ranging from drug design to food processing.

■ ASSOCIATED CONTENT

Ⓢ Supporting Information

The Supporting Information is available free of charge at https://pubs.acs.org/doi/10.1021/acs.cgd.1c00730.

> Pictures of a dilution series of BSA with $CeCl_3$, exemplary SHS and SC fits to BSA and HSA SAXS data, images of HSA-$CeCl_3$ crystals, and SAXS curves of BSA-LaI_3 (PDF)

■ AUTHOR INFORMATION

Corresponding Author

Fajun Zhang − *Institut für Angewandte Physik, Universität Tübingen, 72076 Tübingen, Germany;* ⓘ orcid.org/0000-0001-7639-8594; Email: fajun.zhang@uni-tuebingen.de

Authors

Ralph Maier − *Institut für Angewandte Physik, Universität Tübingen, 72076 Tübingen, Germany;* ⓘ orcid.org/0000-0003-3428-039X

Madeleine R. Fries − *Institut für Angewandte Physik, Universität Tübingen, 72076 Tübingen, Germany;* orcid.org/0000-0002-9643-9215

Cara Buchholz − *Institut für Angewandte Physik, Universität Tübingen, 72076 Tübingen, Germany*

Frank Schreiber − *Institut für Angewandte Physik, Universität Tübingen, 72076 Tübingen, Germany;* orcid.org/0000-0003-3659-6718

Complete contact information is available at:
https://pubs.acs.org/10.1021/acs.cgd.1c00730

Notes

The authors declare no competing financial interest.

REFERENCES

(1) Curry, S.; Mandelkow, H.; Brick, P.; Franks, N. Crystal structure of human serum albumin complexed with fatty acid reveals an asymmetric distribution of binding sites. *Nat. Struct. Biol.* **1998**, *5*, 827−835.

(2) Sugio, S.; Kashima, A.; Mochizuki, S.; Noda, M.; Kobayashi, K. Crystal structure of human serum albumin at 2.5 Å resolution. *Protein Eng., Des. Sel.* **1999**, *12*, 439−446.

(3) Bujacz, A. Structures of bovine, equine and leporine serum albumin. *Acta Crystallogr., Sect. D: Biol. Crystallogr.* **2012**, *68*, 1278−1289.

(4) He, X. M.; Carter, D. C. Atomic structure and chemistry of human serum albumin. *Nature* **1992**, *358*, 209−215.

(5) Klotz, I. M.; Urquhart, J. M. The binding of organic ions by proteins. Comparison of native and of modified proteins. *J. Am. Chem. Soc.* **1949**, *71*, 1597−1603.

(6) Klotz, I. M.; Ayers, J. Interactions of some neutral organic molecules with proteins. *J. Am. Chem. Soc.* **1952**, *74*, 6178−6180.

(7) Wang, S.; Liu, S.; Zhang, Y.; He, J.; Coy, D. H.; Sun, L. Human Serum Albumin (HSA) and Its Applications as a Drug Delivery Vehicle. *Health Sci. J.* **2020**, *14*, 1−8.

(8) Kandagal, P.; Ashoka, S.; Seetharamappa, J.; Shaikh, S.; Jadegoud, Y.; Ijare, O. B. Study of the interaction of an anticancer drug with human and bovine serum albumin: spectroscopic approach. *J. Pharm. Biomed. Anal.* **2006**, *41*, 393−399.

(9) Sułkowska, A.; Równicka, J.; Bojko, B.; Sułkowski, W. Interaction of anticancer drugs with human and bovine serum albumin. *J. Mol. Struct.* **2003**, *651-653*, 133−140.

(10) Maier, R.; Zocher, G.; Sauter, A.; Da Vela, S.; Matsarskaia, O.; Schweins, R.; Sztucki, M.; Zhang, F.; Stehle, T.; Schreiber, F. Protein Crystallization in the Presence of a Metastable Liquid−Liquid Phase Separation. *Cryst. Growth Des.* **2020**, *20*, 7951−7962.

(11) Wolf, M.; Roosen-Runge, F.; Zhang, F.; Roth, R.; Skoda, M. W. A.; Jacobs, R. M. J.; Sztucki, M.; Schreiber, F. Effective interactions in protein-salt solutions approaching liquid-liquid phase separation. *J. Mol. Liq.* **2014**, *200*, 20−27.

(12) Fries, M. R.; Stopper, D.; Braun, M. K.; Hinderhofer, A.; Zhang, F.; Jacobs, R. M.; Skoda, M. W.; Hansen-Goos, H.; Roth, R.; Schreiber, F. Multivalent-ion-activated protein adsorption reflecting bulk reentrant behavior. *Phys. Rev. Lett.* **2017**, *119*, No. 228001.

(13) Fries, M. R.; Conzelmann, N. F.; Günter, L.; Matsarskaia, O.; Skoda, M. W.; Jacobs, R. M.; Zhang, F.; Schreiber, F. Bulk Phase

Behavior vs Interface Adsorption: Specific Multivalent Cation and Anion Effects on BSA Interactions. *Langmuir* **2021**, *37*, 139−150.

(14) Hadichegeni, S.; Goliaei, B.; Taghizadeh, M.; Davoodmanesh, S.; Taghavi, F.; Hashemi, M. Characterization of the interaction between human serum albumin and diazinon via spectroscopic and molecular docking methods. *Hum. Exp. Toxicol.* **2018**, *37*, 959−971.

(15) Gelamo, E.; Tabak, M. Spectroscopic studies on the interaction of bovine (BSA) and human (HSA) serum albumins with ionic surfactants. *Spectrochim. Acta, A* **2000**, *56*, 2255−2271.

(16) Bal, W.; Christodoulou, J.; Sadler, P. J.; Tucker, A. Multi-metal binding site of serum albumin. *J. Inorg. Biochem.* **1998**, *70*, 33−39.

(17) Michnik, A.; Michalik, K.; Kluczewska, A.; Drzazga, Z. Comparative DSC study of human and bovine serum albumin. *J. Therm. Anal. Calorim.* **2006**, *84*, 113−117.

(18) Akdogan, Y.; Reichenwallner, J.; Hinderberger, D. Evidence for water-tuned structural differences in proteins: an approach emphasizing variations in local hydrophilicity. *PLoS One* **2012**, *7*, No. e45681.

(19) Zhang, F.; Weggler, S.; Ziller, M. J.; Ianeselli, L.; Heck, B. S.; Hildebrandt, A.; Kohlbacher, O.; Skoda, M. W. A.; Jacobs, R. M. J.; Schreiber, F. Universality of protein reentrant condensation in solution induced by multivalent metal ions. *Proteins: Struct., Funct., Bioinf.* **2010**, *78*, 3450−3457.

(20) Fries, M. R.; Stopper, D.; Skoda, M. W.; Blum, M.; Kertzscher, C.; Hinderhofer, A.; Zhang, F.; Jacobs, R. M.; Roth, R.; Schreiber, F. Enhanced protein adsorption upon bulk phase separation. *Sci. Rep.* **2020**, *10*, No. 10349.

(21) Da Vela, S.; Braun, M. K.; Dörr, A.; Greco, A.; Möller, J.; Fu, Z.; Zhang, F.; Schreiber, F. Kinetics of liquid−liquid phase separation in protein solutions exhibiting LCST phase behavior studied by time-resolved USAXS and VSANS. *Soft Matter* **2016**, *12*, 9334−9341.

(22) Matsarskaia, O.; Braun, M. K.; Roosen-Runge, F.; Wolf, M.; Zhang, F.; Roth, R.; Schreiber, F. Cation-Induced Hydration Effects Cause Lower Critical Solution Temperature Behavior in Protein Solutions. *J. Phys. Chem. B* **2016**, *120*, 7731−7736.

(23) Matsarskaia, O.; Roosen-Runge, F.; Lotze, G.; Möller, J.; Mariani, A.; Zhang, F.; Schreiber, F. Tuning phase transitions of aqueous protein solutions by multivalent cations. *Phys. Chem. Chem. Phys.* **2018**, *20*, 27214−27225.

(24) Zhang, F.; Skoda, M. W. A.; Jacobs, R. M. J.; Zorn, S.; Martin, R. A.; Martin, C. M.; Clark, G. F.; Weggler, S.; Hildebrandt, A.; Kohlbacher, O.; Schreiber, F. Reentrant Condensation of Proteins in Solution Induced by Multivalent Counterions. *Phys. Rev. Lett.* **2008**, *101*, No. 148101.

(25) Zhang, F.; Zocher, G.; Sauter, A.; Stehle, T.; Schreiber, F. Novel approach to controlled protein crystallization through ligandation of yttrium cations. *J. Appl. Cryst.* **2011**, *44*, 755−762.

(26) Matsarskaia, O.; Roosen-Runge, F.; Schreiber, F. Multivalent ions and biomolecules: Attempting a comprehensive perspective. *ChemPhysChem* **2020**, *21*, 1742−1767.

(27) Zhang, F.; Roth, R.; Wolf, M.; Roosen-Runge, F.; Skoda, M. W. A.; Jacobs, R. M. J.; Sztucki, M.; Schreiber, F. Charge-controlled metastable liquid-liquid phase separation in protein solutions as a universal pathway towards crystallization. *Soft Matter* **2012**, *8*, 1313−1316.

(28) Sober, H. A. *CRC Handbook of Biochemistry: Selected Data for Molecular Biology*; CRC, 1970.

(29) Blanchet, C. E.; Spilotros, A.; Schwemmer, F.; Graewert, M. A.; Kikhney, A.; Jeffries, C. M.; Franke, D.; Mark, D.; Zengerle, R.; Cipriani, F.; Fiedler, S.; Roessle, M.; Severgun, D. I. Versatile sample environments and automation for biological solution X-ray scattering experiments at the P12 beamline (PETRA III, DESY). *J. Appl. Crystallogr.* **2015**, *48*, 431−443.

(30) Baxter, R. J. Percus−Yevick Equation for Hard Spheres with Surface Adhesion. *J. Chem. Phys.* **1968**, *49*, 2770−2774.

(31) Kline, S. R. Reduction and analysis of SANS and USANS data using IGOR Pro. *J. Appl. Cryst.* **2006**, *39*, 895−900.

(32) Menon, S. V. G.; Manohar, C.; Rao, K. S. A new interpretation of the sticky hard sphere model. *J. Chem. Phys.* **1991**, *95*, 9186−9190.

(33) Braun, M. K.; Sauter, A.; Matsarskaia, O.; Wolf, M.; Roosen-Runge, F.; Sztucki, M.; Roth, R.; Zhang, F.; Schreiber, F. Reentrant phase behavior in protein solutions induced by multivalent salts: strong effect of anions Cl$^-$ versus NO$_3^-$. *J. Phys. Chem. B* **2018**, *122*, 11978−11985.

(34) Lee, J.; Timasheff, S. Partial specific volumes and interactions with solvent components of proteins in guanidine hydrochloride. *Biochemistry* **1974**, *13*, 257−265.

(35) Hianik, T.; Poniková, S.; Bágelová, J.; Antalík, M. Specific volume and compressibility of human serum albumin−polyanion complexes. *Bioorg. Med. Chem. Lett.* **2006**, *16*, 274−279.

(36) Braun, M. K.; Wolf, M.; Matsarskaia, O.; Da Vela, S.; Roosen-Runge, F.; Sztucki, M.; Roth, R.; Zhang, F.; Schreiber, F. Strong Isotope Effects on Effective Interactions and Phase Behavior in Protein Solutions in the Presence of Multivalent Ions. *J. Phys. Chem. B* **2017**, *121*, 1731−1739.

(37) Hansen, J.-P.; Hayter, J. B. A rescaled MSA structure factor for dilute charged colloidal dispersions. *Mol. Phys.* **1982**, *46*, 651−656.

(38) Hayter, J. B.; Penfold, J. An analytic structure factor for macroion solutions. *Mol. Phys.* **1981**, *42*, 109−118.

(39) Zhang, F.; Roosen-Runge, F.; Skoda, M. W. A.; Jacobs, R. M. J.; Wolf, M.; Callow, P.; Frielinghaus, H.; Pipich, V.; Prevost, S.; Schreiber, F. Hydration and interactions in protein solutions containing concentrated electrolytes studied by small-angle scattering. *Phys. Chem. Chem. Phys.* **2012**, *14*, 2483−2493.

(40) Reviakine, I.; Johannsmann, D.; Richter, R. P. Hearing what you cannot see and visualizing what you hear: interpreting quartz crystal microbalance data from solvated interfaces. *Anal. Chem.* **2011**, *83*, 8838−8848.

(41) Zhang, B.; Wang, Q. Quartz crystal microbalance with dissipation. *Nanotechnol. Res. Methods Foods Bioprod.* **2012**, 181−194.

(42) Voinova, M. V.; Rodahl, M.; Jonson, M.; Kasemo, B. Viscoelastic acoustic response of layered polymer films at fluid-solid interfaces: continuum mechanics approach. *Phys. Scr.* **1999**, *59*, 391.

(43) Feiler, A. A.; Sahlholm, A.; Sandberg, T.; Caldwell, K. D. Adsorption and viscoelastic properties of fractionated mucin (BSM) and bovine serum albumin (BSA) studied with quartz crystal microbalance (QCM-D). *J. Colloid Interface Sci.* **2007**, *315*, 475−481.

(44) Rojas, E.; Gallego, M.; Reviakine, I. Effect of sample heterogeneity on the interpretation of quartz crystal microbalance data: impurity effects. *Anal. Chem.* **2008**, *80*, 8982−8990.

(45) Roosen-Runge, F.; Zhang, F.; Schreiber, F.; Roth, R. Ion-activated Attractive Patches as a Mechanism for Controlled Protein Interactions. *Sci. Rep.* **2014**, *4*, No. 7016.

(46) Bijelic, A.; Rompel, A. The use of polyoxometalates in protein crystallography An attempt to widen a well-known bottleneck. *Coord. Chem. Rev.* **2015**, *299*, 22−38.

(47) Vliegenthart, G. A.; Lekkerkerker, H. N. W. Predicting the gas−liquid critical point from the second virial coefficient. *J. Chem. Phys.* **2000**, *112*, 5364−5369.

(48) Lindner, P.; Zemb, T. *Neutrons, X-rays, and Light: Scattering Methods Applied to Soft Condensed Matter*; Elsevier North-Holland, 2002.

(49) Hansen, J.-P.; McDonald, I. R. *Theory of Simple Liquids*, 3rd ed.; Academic press, 2006.

(50) Fries, M. R.; Skoda, M. W.; Conzelmann, N. F.; Jacobs, R. M.; Maier, R.; Scheffczyk, N.; Zhang, F.; Schreiber, F. Bulk phase behaviour vs interface adsorption: Effects of anions and isotopes on β-lactoglobulin (BLG) interactions. *J. Colloid Interface Sci.* **2021**, *598*, 430−443.

(51) Kurrat, R.; Prenosil, J.; Ramsden, J. Kinetics of human and bovine serum albumin adsorption at silica−titania surfaces. *J. Colloid Interface Sci.* **1997**, *185*, 1−8.

(52) von Bülow, S.; Siggel, M.; Linke, M.; Hummer, G. Dynamic cluster formation determines viscosity and diffusion in dense protein solutions. *Proc. Natl. Acad. Sci. U.S.A.* **2019**, *116*, 9843−9852.

(53) Jachimska, B.; Wasilewska, M.; Adamczyk, Z. Characterization of globular protein solutions by dynamic light scattering, electro-phoretic mobility, and viscosity measurements. *Langmuir* **2008**, *24*, 6866−6872.

(54) Dockal, M.; Carter, D. C.; Rüker, F. Conformational Transitions of the Three Recombinant Domains of Human Serum Albumin Depending on pH. *J. Biol. Chem.* **2000**, *275*, 3042−3050.

(55) Dockal, M.; Carter, D. C.; Rüker, F. The three recombinant domains of human serum albumin: structural characterization and ligand binding properties. *J. Biol. Chem.* **1999**, *274*, 29303−29310.

(56) Murayama, K.; Tomida, M. Heat-induced secondary structure and conformation change of bovine serum albumin investigated by Fourier transform infrared spectroscopy. *Biochemistry* **2004**, *43*, 11526−11532.

(57) Schomäcker, K.; Mocker, D.; Münze, R.; Beyer, G.-J. Stabilities of lanthanide-protein complexes. *Appl. Radiat. Isot.* **1988**, *39*, 261−264.

(58) Ramberg, K. O.; Engilberge, S.; Skorek, T.; Crowley, P. B. Facile Fabrication of Protein−Macrocycle Frameworks. *J. Am. Chem. Soc.* **2021**, *143*, 1896−1907.

(59) Ohyoshi, E.; Kohata, S. The binding of Yb (III) and Gd (III) to bovin serum albumin by a competitive spectrophotometry. *J. Inorg. Biochem.* **1993**, *52*, 157−163.

(60) Roosen-Runge, F.; Heck, B. S.; Zhang, F.; Kohlbacher, O.; Schreiber, F. Interplay of pH and Binding of Multivalent Metal Ions: Charge Inversion and Reentrant Condensation in Protein Solutions. *J. Phys. Chem. B* **2013**, *117*, 5777−5787.

(61) Blaber, M.; Zhang, X. J.; Matthews, B. W. Structural basis of amino acid alpha helix propensity. *Science* **1993**, *260*, 1637−1640.

(62) George, A.; Wilson, W. W. Predicting protein crystallization from a dilute solution property. *Acta Crystallogr., Sect. D: Biol. Crystallogr.* **1994**, *50*, 361−365.

(63) Schmit, J. D.; Dill, K. Growth rates of protein crystals. *J. Am. Chem. Soc.* **2012**, *134*, 3934−3937.

(64) Whitelam, S. Control of Pathways and Yields of Protein Crystallization through the Interplay of Nonspecific and Specific Attractions. *Phys. Rev. Lett.* **2010**, *105*, No. 088102.

(65) Staneva, I.; Frenkel, D. The role of non-specific interactions in a patchy model of protein crystallization. *J. Chem. Phys.* **2015**, *143*, No. 194511.

(66) Jelsch, C.; Longhi, S.; Cambillau, C. Packing forces in nine crystal forms of cutinase. *Proteins: Struct., Funct., Genet.* **1998**, *31*, 320−333.

(67) Rosenbach, H.; Victor, J.; Borggräfe, J.; Biehl, R.; Steger, G.; Etzkorn, M.; Span, I. Expanding crystallization tools for nucleic acid complexes using U1A protein variants. *J. Struct. Biol.* **2020**, *210*, No. 107480.

(68) Elbasir, A.; Mall, R.; Kunji, K.; Rawi, R.; Islam, Z.; Chuang, G.-Y.; Kolatkar, P. R.; Bensmail, H. BCrystal: an interpretable sequence-based protein crystallization predictor. *Bioinformatics* **2020**, *36*, 1429−1438.

(69) Majorek, K. A.; Porebski, P. J.; Dayal, A.; Zimmerman, M. D.; Jablonska, K.; Stewart, A. J.; Chruszcz, M.; Minor, W. Structural and immunologic characterization of bovine, horse, and rabbit serum albumins. *Mol. Immunol.* **2012**, *52*, 174−182.

(70) Wang, Q.; Xue, C.; Qin, Y.; Zhang, X.; Li, Y. The fabrication of protein microbubbles with diverse gas core and the novel exploration on the role of interface introduction in protein crystallization. *Colloids Surf., A* **2020**, *589*, No. 124471.

(71) Rosseneu-Motreff, M.; Blaton, V.; Declercq, B.; Vandamme, D.; Peeters, H. Size and Shape Determination of Native and Detatted Bovine Serum Albumin Monomers: I. Chemical Characterization of Lipids Bound to Native and Defatted-Bovine Serum Albumin Monomers. *J. Biochem.* **1970**, *68*, 369−377.